# Chapter 14

# Life in Crowded and Disordered Environments

"Nobody goes there anymore. It's too crowded." -Yogi Berra

**Chapter Overview: In Which We Reexamine the Picture of Dilute Solutions and Account for Cellular Crowding**

The cellular interior is so crowded that the distance between neighboring proteins is comparable to protein size itself. Similarly, the cell membrane is richly inhabited with large numbers of proteins of different types in a lipid background that is highly varied. This means that the material environment of cells is far different from the conditions found in most biochemical experiments and featured in many of the models described so far. In particular, we have ignored the effects of this crowding by exploiting simple ideas about binding which exploit the "dilute-solution" limit. Similarly, our treatment of diffusive kinetics has been built around a random-walk picture in which molecules are free to wander unencumbered by interactions with neighboring walkers. This chapter examines how crowding alters both equilibria and kinetics and examines some simple toy models of these effects.

## 14.1 Crowding, Linkage and Entanglement

Much of the substance of our quantitative story of cells has thus far centered on different ways of viewing binding and diffusion problems. Binding and diffusion are central to the biochemical reactions that are the engine of cellular life. However, many of the assumptions which are hidden behind our use of these concepts seem to be at odds with the way cells really work. Two of the key assumptions that have been behind the scenes in much of what we have done are: i) the assumption of *ideality* in which it is supposed that the molecules of interest are sufficiently dilute that they do not interact either through direct contact

or even through longer range potentials, and ii) the assumption of *homogeneity* which posits that the environment at one place is just like it is somewhere else. The present chapter examines how to relax these two assumptions and to ask what new insights into biological structure and function then emerge.

Cellular life is colored by various broad classes of phenomena which are at odds with the assumptions of ideality and homogeneity. One of the simplest facts of cellular life that contradicts the ideality assumptions favored so far in the book is the intense crowding of the cellular interior. A mean spacing of less than 10 nm between proteins is a conservative estimate of the extent of crowding, a fact that we will show has implications both for equilibria as well as kinetics. This mean spacing should be contrasted with the roughly 100 nm spacing between molecules that would be found in the "high" concentration of an *in vitro* experiment taking place at millimolar concentrations.

Examination of cells using either light microscopy or an electron microscope reveals a wide variety of organized structures which demonstrate that the homogeneity assumptions we have invoked so far are often inappropriate. What is revealed is a heterogeneous environment characterized by *linked* polymer networks such as the actin network that crisscrosses the leading edge of motile cells or the peptidoglycan network that confers bacterial shape. In addition, the presence of organelles such as are found in eukaryotes reveal even more subtle and intriguing features such as different lipid compositions for adjacent organelles such as the endoplasmic reticulum and the Golgi apparatus.

This chapter probably raises more questions than it answers, but it is built around two broad thrusts: a) how should we amend our treatment of binding and interaction to account for crowding effects on biochemical equilibria, and b) how are the diffusive dynamics seen in cells different than that found in dilute solutions?

### 14.1.1 The Cell is Crowded

The ability to experimentally perform a quantitative census of cells as was described in chap. 2 has transformed our understanding of living matter. Experiments like those shown in figs. 2.3 (pg. 63) and 2.10 (pg. 77) make it possible to count up the number of copies of many of the different proteins that make cells function. In addition, such experiments have served as the inspiration for a new generation of iconic illustrations such as fig. 2.2 (pg. 62) whose aim is "to help imagine biological molecules in their proper context: packed into living cells." (Goodsell, 1998) In biochemical reactions in the laboratory, much care is taken to insure that features such as the concentration and the charge state (as reflected in the pH and the ionic strength) mimic those of living cells. On the other hand, many of these experiments ignore the need to "correct for extract dilution with molecular crowding", a dictum elevated to the status of a biochemical commandment by Arthur Kornberg (Kornberg, 2000).

To get a sense of the crowded nature of the cellular interior, we return to our estimates of section 2.1.2 (pg. 59), where we took stock of the census of a bacterium. Hidden within those calculations is a simple way to view the extent

of crowding within the cellular interior. The simplest estimate is to imagine a bacterium as a cube with edge length of 1000 nm (i.e. 1 $\mu m$). As shown in fig. 2.2, we estimated that there are roughly several million proteins within an *E. coli* cell. For simplicity, imagine that there are $10^6$ such proteins in the cytoplasm of our bacterium. This means that in our hypothetical cubic bacterium we can line them up 100 on a side in all three directions. This means that the mean center to center spacing is 10 nm. To further simplify our estimate, now imagine that our proteins are all spheres with a radius of 2 nm. What this means is that the "solution" between proteins is slightly more than 5 nm thick. The picture this estimate paints of the cellular interior is one in which the diluteness and homogeneity of ideal solution theory is drastically overthrown. However, crowding is more diverse and subtle than the mere fact that there are lots of proteins squashed together. One way in which this crowding is more subtle is in the form of the many networks of filamentous molecules that crisscross cells, a topic we explore presently.

### 14.1.2 Macromolecular Networks: The Cytoskeleton and Beyond

As will be shown below, crowding of spheres is one instructive way to understand excluded volume effects and the depletion forces they engender. However, these ideas fall short as we try to more closely approximate structures and conditions within living organisms. This is because most of the components responsible for structural organization and mechanical properties of living cells and organisms are better approximated by elastic beams rather than spheres. In chap. 10, we considered the properties of individual filaments but now in our attempt to effect a more realistic treatment of living conditions we must consider what happens when large numbers of filaments are densely crowded together. This happens not only within cells, but also outside of cells in extracellular matrix. Indeed, the implausibly tall size of animals and green plants can only be maintained against gravity because of the remarkable properties of filamentous structures of the extracellular matrix.

Aligned filament structures are commonly seen in organisms. Some examples are shown in fig. 14.1. We have already seen how parallel bundles of actin filaments and microtubules are used in building cell surface projections that resist buckling (see chap. 10) such as the microvilli seen in fig. 14.1(A). Bundles of filaments are also found within cells contributing to intracellular traffic. A dramatic example of this is the aligned bundles of microtubules and intermediate filaments in the axon of a neuron as shown in fig. 14.1(B). Aligned filaments of extracellular matrix shown in fig. 14.1(C) give our tendons and ligaments their remarkable resistance against shearing. The alignment of collagen in tendons can be easily seen even at the level of light microscopy. Similar alignment of cellulose fibers in the plant extracellular matrix allows, as shown in fig. 14.1(D), trees to grow against gravity to be up to several hundred meters tall.

Although formation of aligned filament bundles can greatly enhance the strength and mechanical properties beyond that of individual filaments, a short-

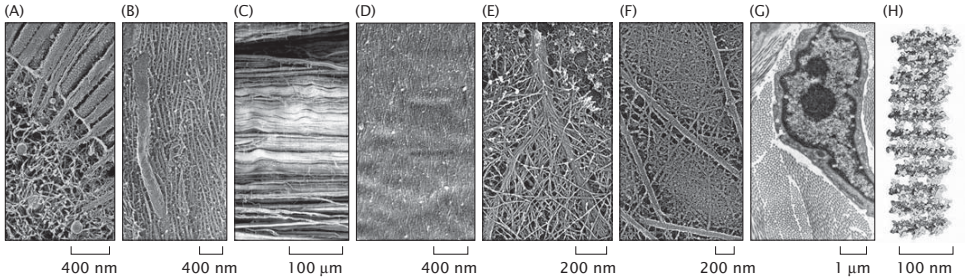


Figure 14.1: Gallery of filamentous network architectures found in cells and extracellular matrix. (A) The upper edge of an intestinal epithelial cell reveals tightly packed bundles of actin in the microvilli and a less organized but still dense actin meshwork just below the membrane. (B) Within the axon of a nerve aligned and tightly packed bundles of neurofilaments and microtubules allow the axon to grow very long and serve as tracks for transporting organelles such as mitochondria. (C) In animal ligaments such as this one from a rat, aligned collagen bundles resist shear stresses. (D) The cell wall of plants is made of aligned bundles of cellulose for organisms ranging from this tiny weed *Arabidopsis* to the mighty Redwood. (E) At the leading edge of a moving cell, actin filaments in webs and bundles grow to push the membrane forward. (F) Animal tissues made of epithelial cells usually include a basement membrane lining underneath the cells to improve the mechanical strength of the tissue. The basement membrane is not a phospholipid membrane but rather a felt-like mat of collagen, proteoglycans and other filamentous molecules. (G) Cells such as the fibroblast shown here navigate through densely packed extracellular matrix. In this thin section, collagen fibrils have been sliced in several different orientations revealing their regular packing. (H) The cell wall of gram-positive bacteria is constructed of filamentous strands of sugars crosslinked by unusual peptides. This atomic model shows one possible orientation of the filaments. (A, F, courtesy of John Heuser; B, adapted from N. Hirokawa, J. Cell Biol., 94:129, 1982; C, adapted from P. P. Provenzano *et al.*, J. Orthop. Res., 20:975, 2002; D, adapted from D. H. Burk and Z. H. Ye, Plant Cell, 14:2145, 2002; E, adapted from T. M. Svitkina *et al.*, J. Cell Biol., 160:409, 2003; G, adapted from P. C. Cross and K. L. Mercer, Cell and Tissue Ultrastructure, New York: W. H. Freeman and Company, 1993; H, adapted from S. O. Meroueh *et al.*, Proc. Nat. Acad. Sci., 103:4404, 2006.)

coming of this organizational motif is that it is extremely anisotropic. In many cases cells must be able to resist mechanical insults coming from all directions, not just those conveniently aligned with the bundle axis. To build mechanically strong three-dimensional structures, cells often crosslink their filaments into networks where the angle of intersection between neighboring filaments may be quite large. Again, network organizations are found throughout nature made of many types of filaments. In fig. 14.1(E), we see the branched network of actin filaments at the leading edge of a crawling cell. Extracellular connective tissue such as the basement membrane shown in fig. 14.1(F) and the collagen rich tissue shown in fig. 14.1(G) can also be arranged to resist shear and stretching forces at multiple orientations. The rigid cell walls of bacterial cells also follow this structural theme where long, fibrils made of chains of sugars are crosslinked by small peptides creating a three-dimensional structure that resists external stresses. An example is shown in fig. 14.1(H).

Cells not only allow filament bundling and superstructural organization to happen but encourage it with crosslinking proteins that tie filaments together. Spontaneous alignment alone will give a mixed orientation of polar filaments, but in many of the examples seen in cells the filaments are all pointing in the same direction. This cannot arise from entropy alone, but rather emerges from local nucleating sites to make sure everything grows in the same direction or exploitation of motor proteins to sort out filaments based on their orientations. This will be further discussed in chap. 16. A higher resolution image of filamentous organization at the leading edge of a motile cell is shown in fig. 14.2. One of the intriguing features of this organization is that it varies as a function of distance from the leading edge itself. In chap. 15, we will explore how the time-dependent growth of actin filaments can lead to this organization.

### 14.1.3 Crowding on Membranes

In addition to the important role of crowding in the three-dimensional setting of the cellular interior, crowding is also a fact of life in the cell membrane. The existence of such crowding in cell membranes was already illustrated in fig. 11.10 (pg. 573) which illustrates how membrane proteins in mitochondria can be manipulated by the application of an electric field. The result of the application of a field is to segregate the membrane proteins to one side of the membrane as shown in the electron micrograph of freeze-fractured membranes. This image and others demonstrate the large fraction of membrane devoted to membrane proteins. Indeed, in the case of the mitochondria, more than 50 percent of the membrane mass is donated by proteins. Interesting measurements of the relative mass of phospholipids and membrane proteins are reported in Mitra *et al.* (2004).

Just as simple estimates on protein concentrations in the cytoplasm reveal a mean spacing comparable to protein size, similar estimates can be carried out for the cell membrane as well. To see this, we recall that the membrane area for a bacterium like *E. coli* is roughly 6 $\mu m^2$ and that both the inner and outer membranes are home to roughly 500,000 proteins. This tells us that the area

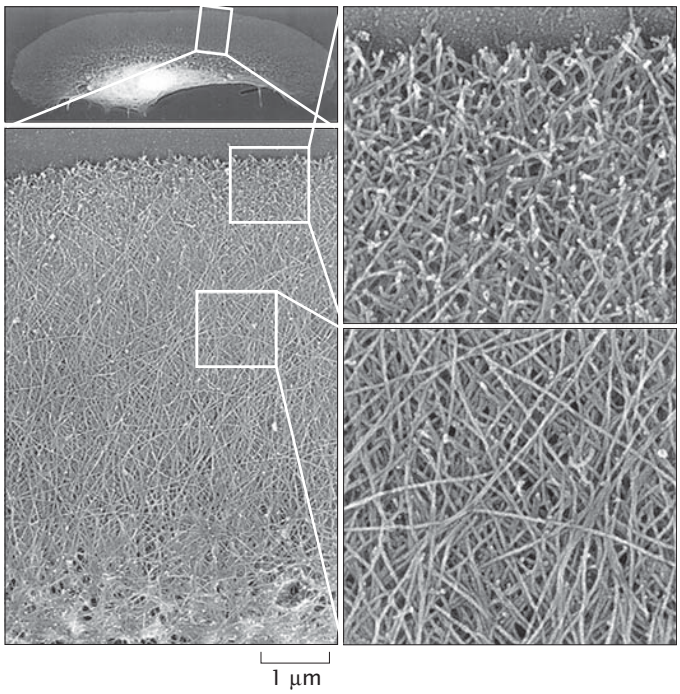


Figure 14.2: Organization of actin filaments at the leading edge of a crawling cell. This fish skin keratocyte was moving upward at the time that it was fixed. Its membrane was stripped off and the filamentous structures imaged after being coated with a very thin layer of platinum. The large white blob towards the bottom of the cell shows the location of the nucleus and the membranous organelles. The area within the white box is blown up below. Essentially all of the filaments are actin. Two regions are shown at still higher magnification on the right. At the top, near the front edge of the cell, the actin filaments are short and frequently branched. Further back, individual actin filaments are longer and overlaid at nearly random angles. (Adapted from T. M. Svitkina *et al.*, J. Cell Biol., 139:397, 1997.)

per protein is roughly 10 $nm^2$, or that the typical distance between two proteins is of order 3 nm. The cell membrane is tightly packed indeed.

### 14.1.4 Consequences of Crowding

So far, we have examined the structural features of the crowded environment of cells. We have seen that this crowded structure which serves as the backdrop for the bustling biochemical metropolis of the cell is quite different from the dilute and homogeneous environments of solution biochemistry. What are the consequences of this crowding for cells? We explore two broad classes of consequence arising from this crowding, namely, how equilibrium binding is modified by crowding and how diffusive processes are altered as a result of the tight packing of cells.

**Crowding Alters Biochemical Equilibria**

The first broad category of effects that can be blamed on crowding are the modifications that take place in equilibria. For example, crowding can alter the equilibrium state of a system relative to the dilute limit of solution biochemistry. In chap. 6, we illustrated how statistical mechanics can be used to compute binding curves which tell us the occupancy of a receptor, for example, as a function of the concentration of ligands. However, such results are modified in various ways by the presence of "passive" crowding agents. What this means concretely is that the binding probability for some substrate as a function of the substrate concentration will be enhanced relative to the case in which there are no crowding agents. A second intriguing outcome of the existence of crowding is the onset of new types of entropic forces which have nothing to do with van der Waals forces or charges. These entropic forces are known alternately as "excluded-volume forces" or "depletion interactions" and can have the counterintuitive effect of apparently introducing "order".

An example of how binding may be altered by crowding effects is shown in fig. 14.3. In this case the measurement examines accessory protein complexes associated with DNA replication in bacteriophage. In particular, this data shows the effect of crowding molecules on the likelihood of binding of gene products 45 (sliding clamp) and 44/62 (clamp-loader) which then themselves bind to the DNA polymerase and enhance its activity. These four molecules together suffice to produce leading-strand synthesis in DNA replication. The crowding agent used in this case is polyethylene glycol with an average mass of 12 kDa. When they are bound in the replication complex, these two phage proteins have the effect of increasing the activity of the T4 DNA polymerase. The rate of ATP hydrolysis by the clamp loader (gp44/62) is used as a readout of the extent of binding of these accessory proteins and this is what is plotted in the figure for the case in which the concentration of gp44/62 is titrated at fixed concentration of gp45. As a control, it was demonstrated that changing the concentration of crowding molecules did not by itself change the catalytic activity of the DNA polymerase. The data presented in this figure is but one example of a widespread phenomenon in which the addition of inert crowding molecules shifts biochemical

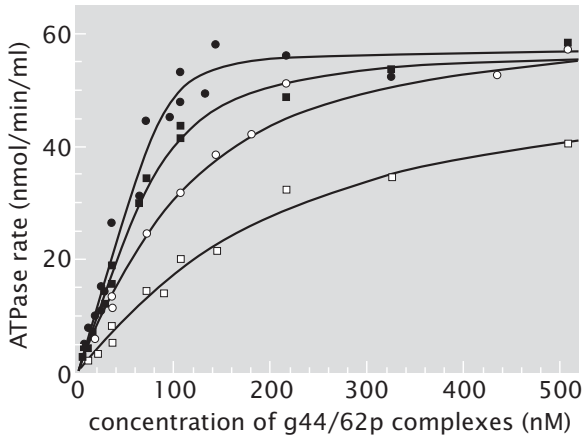


Figure 14.3: ATPase rate associated with T4 DNA replication. The different curves measure the ATPase rate as a function of the g44/62 protein concentration as measured using different concentrations of polyethylene glycol (PEG) as a crowding agent. The concentration of PEG in going from the bottom to the top curve are 0%, 2.5%, 5% and 7.5% weight percent. (Adapted from T. C. Jarvis *et al.*, J. Biol. Chem., 265:15160, 1990.)

equilibria.

**Crowding Alters the Kinetics Within Cells**

Not only does crowding alter equilibrium properties, it also can significantly impact a variety of dynamical processes within cells. A simple starting point is the question of how diffusion is altered in cells relative to in dilute solutions. One way to examine this question is to use fluorescence recovery after photobleaching (FRAP) as introduced in section 13.1.2 (pg. 675). The idea is to fluorescently label some macromolecule of interest within the cell and to measure the diffusive dynamics of these proteins after some region within the cell has been photobleached. An example of such an experiment is shown in fig. 13.7 (pg. 676). The outcome of FRAP experiments is a measure of the slowing down of diffusion relative to its dilute-solution values as shown in fig. 14.4, where the relative diffusion coefficient in the cell interior with respect to water is plotted as a function of the size of the diffusing particle. These curves show a fourfold decrease in the diffusion constant with an even stronger effect for larger molecules.

A second interesting way in which diffusive dynamics is altered is revealed by examining the dynamics of membrane proteins at the cell surface. Video microscopy in which individual membrane proteins are followed reveals that the diffusive trajectories suffered by these molecules are quite distinct from the traditional two-dimensional random walk that would be expected of free

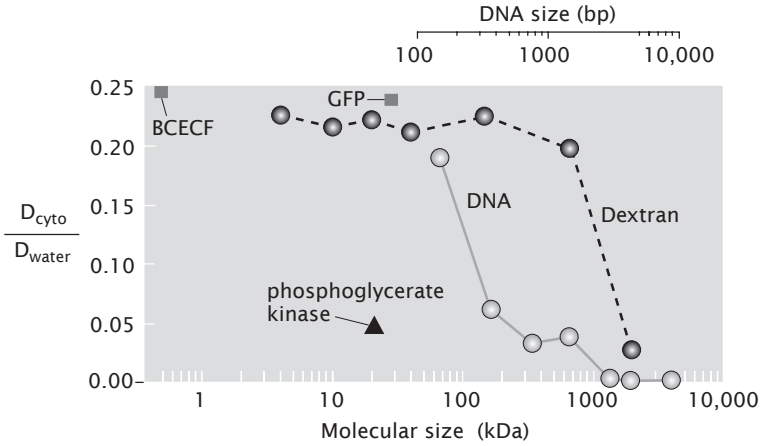


Figure 14.4: Diffusion constants in cells. The plot shows the ratio of the measured cellular diffusion constant to that for the same molecule in water for several different molecules including a series of DNA molecules of different size. (Adapted from A. S. Verkman, Trends Biochem. Sci., 27:27, 2002.)

diffusion. In particular, what is observed are several different categories of phenomena. One class of motions illustrated in fig. 14.5 is episodes of free diffusion punctuated by transient association with other membrane proteins. A related class of diffusive motions reveals free diffusion within what appear to be two-dimensional cages followed by escape to some adjacent cage followed by more localized diffusion. The same phenomenon has been observed in three-dimensional diffusion both for labeled RNAs inside of living cells and for various kinds of tracer particles in three-dimensional filamentous networks constructed *in vitro*. As in the two-dimensional case, individual trajectories are characterized by rapid diffusion within apparent cages, interspersed by rare jumps from one cage to another. In both cases, the observed dynamics may be complicated by the fact that the cages themselves are undergoing dynamic remodeling.

The key point of this section has been to use a few examples of real world data to illustrate how both binding and kinetics are modified by crowding. In the remainder of the chapter, we explore a variety of highly simplified models which illustrate mechanisms where crowding agents have the effect of: altering equilibrium binding curves, inducing entropic forces between particles that are indifferent to each other in dilute solution and slowing down diffusion.

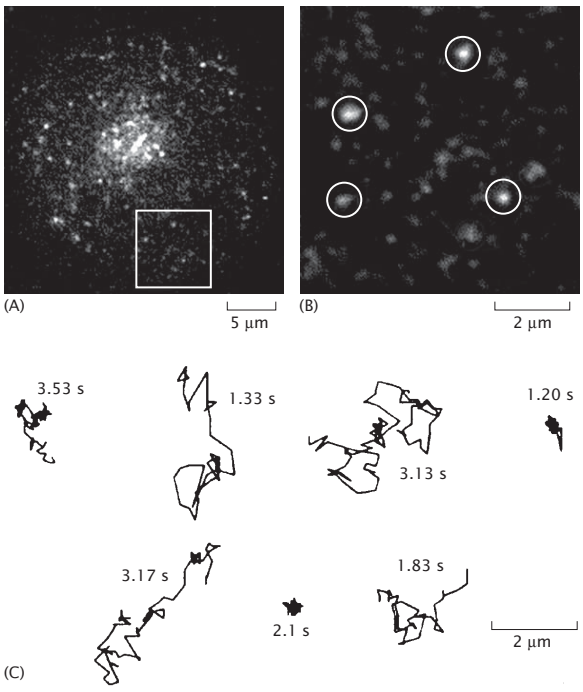


Figure 14.5: Single-molecule measurements for diffusion of membrane-associated proteins. (A) Cells were transfected with a construct encoding GFP fused to a membrane protein Lck. In the fluorescence microscope, the cells appear to be covered with randomly distributed spots. (B) In a magnified view of the region bounded by the box in (A), individual molecules can be clearly seen (circles). Their movement can be tracked over time by video microscopy. (C) A series of tracks measured for individual molecules ranging over total times of about 1 to 3.5 seconds show very heterogenous individual behavior. Some molecules appear to be trapped and nearly stationary, while others travel long distances. (Adapted from A. D. Douglass and R. Vale, Cell, 121:937, 2005.)

## 14.2 Equilibria in Crowded Environments

### 14.2.1 Crowding and binding

In chap. 6, we considered the statistical mechanics of binding of a ligand to a protein using a lattice model. This approach can be extended to the case when the solution contains crowding agents, molecules that do not interact with the ligand or the protein but simply take up space. We consider the effect of crowding molecules on the probability that the receptor's binding site is occupied by the ligand.

**Lattice Models of Solution Provide a Simple Picture of the Role of Crowding in Biochemical Equilibria**

To simplify matters we once again assume that the reaction volume is divided up into $\Omega$ cells of volume $v$ as shown in fig. 14.6. Each of the elementary cells in the lattice model of the solution is either empty (which really means occupied by a solvent molecule), occupied by a ligand or occupied by one of the "crowding" molecules. The total number of ligands and crowding molecules in the reaction volume $\Omega v$ are $L$ and $C$, respectively, as shown in fig. 14.6. If we consider the situation where in solution there are only ligand and crowding molecules present, then in this simple lattice model of the solution, the partition function is

$$Z_{\rm sol}(L,C) = \frac{\Omega!}{L!C!(\Omega - L - C)!} e^{-\beta L \epsilon_L^{\rm sol}} e^{-\beta C \epsilon_C^{\rm sol}} \ , \tag{14.1}$$

where $\epsilon_L^{\rm sol}$ and $\epsilon_C^{\rm sol}$ are the energies of the ligand and crowding molecules in solution. The combinatorial factor in eqn. 14.1 simply counts the number of ways of distributing $L$ ligands and $C$ crowding molecules among the $\Omega$ cells that make up the reaction volume.

Given this model of the solution, we now ask about the probability that the receptor in solution will be bound by a ligand and how this probability depends upon the concentration of both ligand and crowding molecules. The receptor can be in one of two states: either it has the ligand bound, or not. The weights of these two states are $Z_{\rm sol}(L-1,C)\exp(-\beta\epsilon_L^{\rm b})$ and $Z_{\rm sol}(L,C)$, respectively; $\epsilon_L^{\rm b}$ is the energy of the ligand bound to the protein. The probability that the ligand will be bound to the protein is therefore,

$$p_{\rm bound} = \frac{Z_{\rm sol}(L-1,C)e^{-\beta\epsilon_L^{\rm b}}}{Z_{\rm sol}(L-1,C)e^{-\beta\epsilon_L^{\rm b}} + Z_{\rm sol}(L,C)} \ . \tag{14.2}$$

If we divide the numerator and denominator of the above equation by $Z_{\rm sol}(L-1,C)\exp(-\beta\epsilon_L^{\rm b})$ and make the additional assumption that $\Omega - L - C \gg 1$, the equation takes on a simple form,

$$p_{\rm bound} = \frac{1}{1 + \frac{\Omega - L - C}{L} e^{\beta \Delta\epsilon_L}} \ , \tag{14.3}$$

where $\Delta\epsilon_L \equiv \epsilon_L^{\rm b} - \epsilon_L^{\rm sol}$ is the change in the energy of the ligand in going from solution to the receptor.

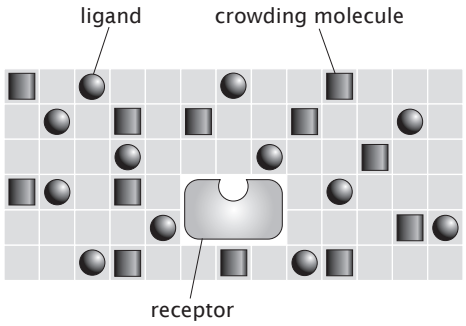


Figure 14.6: Lattice model of crowding and its effect on ligand-protein binding. The reaction volume is occupied by solvent molecules, crowding molecules and ligands. A single ligand can bind to the protein.

From eqn. 14.3 we conclude that the crowding molecules will have an appreciable effect on the probability that a ligand is bound to the protein only in the limit when $C$ is comparable to $\Omega$ (we assume that the number of ligands is small, $L \ll \Omega$). Since the effect of $C$ is to effectively reduce the volume in which the ligands can distribute themselves, we see that an increase in $C$ leads to an increase in $p_{\rm bound}$. This is illustrated in fig. 14.7 where $p_{\rm bound}$ is plotted for a number of different concentrations of the crowding molecules.

A more sophisticated lattice model treatment of crowding and binding allows us to reflect concretely on the data already introduced in fig. 14.3. The theoretical curves shown in that figure are fits to binding curves like those used throughout the book and they yield the dissociation constant as a function of PEG concentration. The resulting dissocation constants are plotted in fig. 14.8. Qualitatively, what this data shows is that as the concentration of crowding agent is increased, the dissocation constant decreases meaning that the binding reaction is more favorable. Our interest is in exploiting simple models to give an intuitive sense of the origins of such data.

To model the PEG dependence of the dissociation constant we make use of the lattice model of crowding described above. The new twist to the story is that the depletant molecules (PEG) are considerably smaller (12 kDa) than the protein complex (gene product 44/62 with a mass of 164 kDa) whose binding is being affected. To account for the size difference, in the lattice model of the solutions we assume that the protein takes up $r$ boxes, where a box can accommodate a single PEG molecule. To further simplify the combinatorics we assume that the reaction volume is broken up into $\Omega$ large boxes, each consisting of $r$ smaller boxes, as shown in fig. 14.9. The proteins take up the larger boxes while the PEG takes up unoccupied smaller boxes. A more detailed calculation

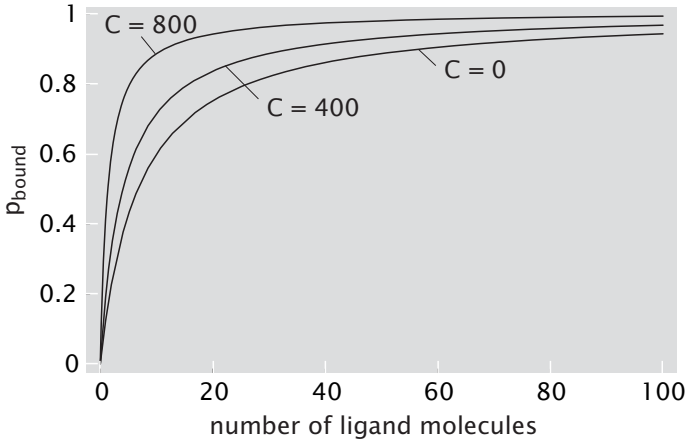


Figure 14.7: Probability of protein binding site occupied by a ligand for a number of different concentrations of the crowding molecules. The reaction volume is $\Omega = 1000$ and $\Delta\epsilon_L = -5\ k_BT$.

would allow the protein to take up any available square region $r$ boxes in size.

For this situation the partition function of the solution of $L$ proteins and $C$ crowding molecules is given by

$$Z_{\text{sol}}(L, C) = \frac{\Omega!}{(\Omega - L)!L!} \frac{(r\Omega - rL)!}{(r\Omega - rL - C)!C!} e^{-\beta L \epsilon_L^{\text{sol}}} e^{-\beta C \epsilon_C^{\text{sol}}} \tag{14.4}$$

which reduces to eqn. 14.1 when $r = 1$. The probability of the protein bound to its receptor can now be computed just as we did for the case when the crowding molecules and the ligands were assumed to be of the same size. In particular, we construct a ratio in which the numerator is the statistical weight of the bound states and the denominator sums over the statistical weights of all states just as we did in eqn. 14.3. This results in a probability of binding of the form

$$p_{\text{bound}} = \frac{1}{1 + \frac{Z_{\text{sol}}(L,C)}{Z_{\text{sol}}(L-1,C)} \exp(\beta\Delta\epsilon_L)} = \frac{1}{1 + \frac{\Omega}{L}(1 - \phi_C)^r \exp(\beta\Delta\epsilon_L)} \tag{14.5}$$

where $\phi_C = \frac{C}{r\Omega}$ is the volume fraction of the crowding molecules in solution. To obtain the last equality we assumed that $L \ll \Omega$, i.e. the volume fraction of the binding proteins is much less than one, and we repeatedly made use of the formula $(N + r)!/N! \approx N^r$ which holds for $N \gg r$.

By comparing eqn. 14.5 to eqn. 6.110 (pg. 346) we can read off the volume-fraction dependent dissociation constant and we find that

$$\frac{K_d(\phi_C)}{K_d(\phi_C = 0)} = (1 - \phi_C)^r. \tag{14.6}$$

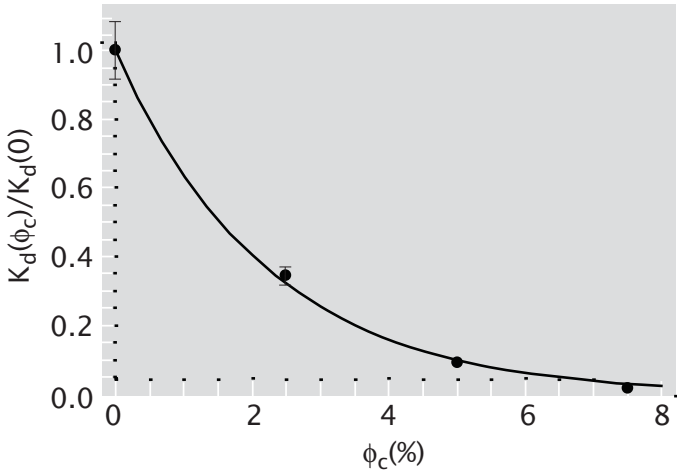


Figure 14.8: Dissociation constant as a function of crowding. Comparison of theory (full line) and experiment (filled circles) for binding in the presence of crowding agents. Measured values of the dissociation constant for gp44/62 and gp45 components of T4 DNA replication complex as a function of PEG concentration measured in percent volume fraction. The theoretical curve is obtained by fitting eqn. 14.6 for the effective size ratio $r$ of the protein components to the PEG 12000 molecules. (Adapted from T. C. Jarvis *et al.*, J. Biol. Chem., 265:15160, 1990.)

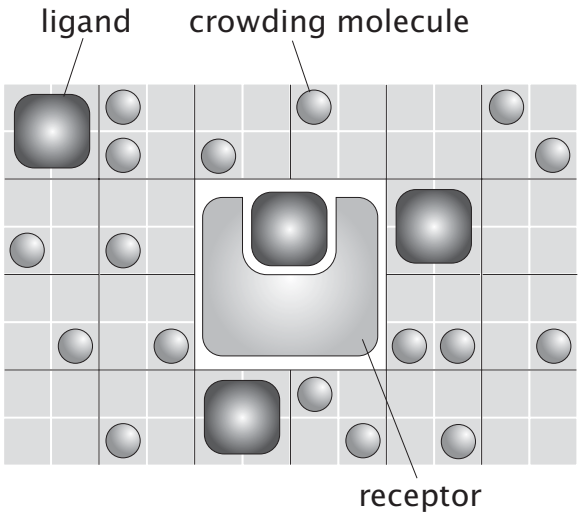


Figure 14.9: Lattice model for large ligands. This lattice model describes binding in the presence of crowding agents where the size of the crowder is different from that of the ligands. This is represented using different size boxes for the crowder and the ligand.

In fig. 14.8 we compare this formula to the data for the gp44/62 protein complex from the T4 bacteriophage. The theoretical curve in the figure results from a best fit to the data using the parameter $r$ which is a measure of the relative "size" of the ligands and the crowder. From *a priori* knowledge of the masses of both the ligands and the crowders, a first guess is that $r \approx 15$, while a best fit yields the value $r = 45$.

The treatment given here only scratches the surface of the way in which crowding agents alter biochemical equilibria. The model introduced here is a caricature of crowding effects and neglects a variety of important features, one of which is indicated schematically in fig. 14.10. More generally, as written the models presented in this section ignore the real "excluded volume" effect in which particles effectively take up more space than their physical volume, and the amount of space they occupy depends upon their overall concentration! The implications of this idea for particle interactions will be taken up in section 14.2.3.

### 14.2.2 Osmotic Pressures in Crowded Solutions

#### Osmotic Pressure Reveals Crowding Effects

One interesting outcome of the presence of proteins and ions in the cellular interior is that they induce an osmotic pressure. Experiments on concentrated

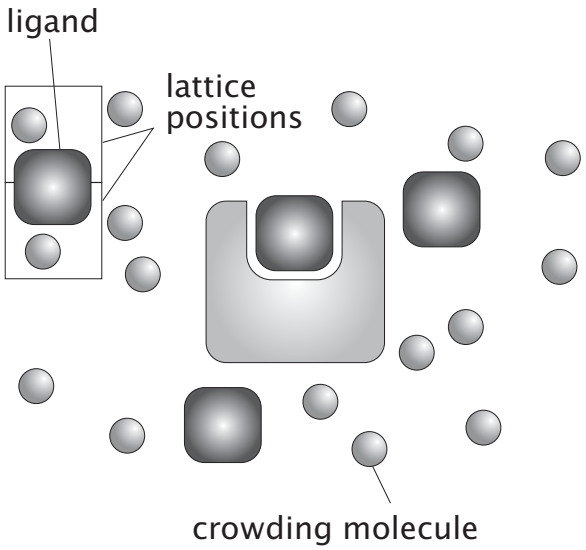


Figure 14.10: Limitations of the lattice model of crowding. This figure shows an allowed configuration for a ligand that is artificially *forbidden* in the lattice model.

solutions of proteins such as hemoglobin can shed light on this phenomenon. An example of such data that reveals the nonlinear dependence of the osmotic pressure on the protein concentration is shown in fig. 14.11. We can think about these data using the lattice model of a crowded solution introduced above. At low concentrations the pressure depends linearly on the amount of hemoglobin present as described by the van't Hoff formula discussed in section 6.2.3 (pg. 337). As the hemoglobin solution becomes concentrated the interactions between the molecules become important and lead to deviations from the simple law.

For the case of a concentrated solution of hemoglobin we employ a lattice model which consists of two species of molecules: filled boxes correspond to hemoglobin molecules and the empty boxes represent the solvent. The partition function for this model is

$$Z_{\rm sol}(H,\Omega) = \frac{\Omega!}{H!(\Omega-H)!} e^{-\beta H \epsilon_H^{\rm sol}} \ , \tag{14.7}$$

This is nothing but eqn. 14.1, where now $H$, the number of hemoglobin molecules, takes the place of the crowding agent $C$, and $L = 0$.

The osmotic pressure $p$ in the lattice model can be computed by considering the change in free energy, $G = -k_B T \ln Z_{\rm sol}$, of the system when its total volume decreases by a single cell of volume $v$. Setting the work equal to the change in

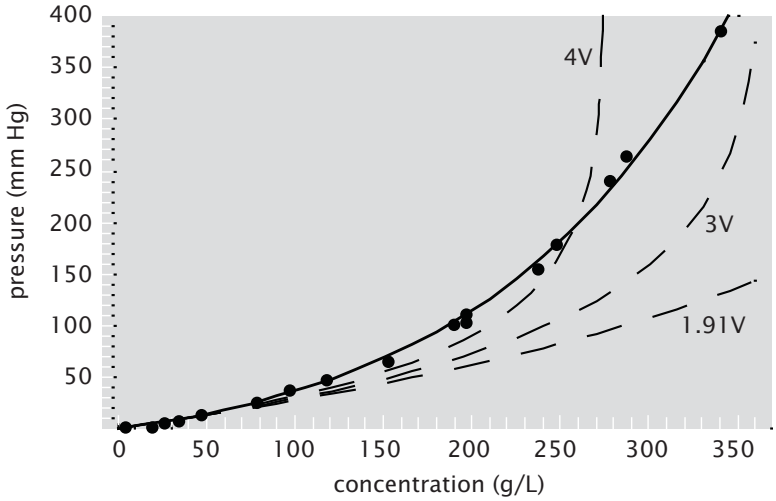


Figure 14.11: Osmotic pressure of a concentrated solution of hemoglobin at 0°C. Full circles are the experimental data points. The dashed lines are predictions of the lattice gas, while the full line is the pressure of a gas of hard spheres, each sphere having volume $V$ corresponding to a diameter of 5.8 nm. The labels on the curves indicate the volume of a single box in the lattice model. (Adapted from P. D. Ross and A. P. Minton, J. Mol. Biol., 112:437, 1977.)

free energy,

$$pv = G(\Omega - 1) - G(\Omega) = -k_B T \ln \frac{Z_{\rm sol}(H, \Omega - 1)}{Z_{\rm sol}(H, \Omega)} \ , \tag{14.8}$$

leads to an expression for the pressure

$$p = \frac{k_B T}{v} \ln \frac{\Omega}{\Omega - H} \tag{14.9}$$

where we have made use of eqn. 14.7. We can rewrite this equation in terms of the concentration of the hemoglobin molecules, $[H] = \frac{H}{\Omega v}$, as

$$p = -\frac{k_B T}{v} \ln(1 - [H]v) \ . \tag{14.10}$$

In fig. 14.11 we compare the pressure predicted by the lattice model with experimental data. Note that the only free parameter in the model is the volume of a single box on the lattice, namely the parameter $v$. To make the comparison concrete, we convert the experimentally determined concentration, which has units $g/l$, to a molar concentration. To do so, we divide by the mass of a single hemoglobin molecule, $m_{\rm Hemoglobin} \approx 68$ kDa. We see that the lattice model reproduces the non-linearity and the right scale of the pressure when we use $v$ which is comparable to the size of a hemoglobin molecule as determined from X-ray scattering.

Despite the favorable qualitative features of the lattice model, it still does not give an entirely satisfactory description of the observed osmotic pressure. Happily, there is a long tradition in statistical physics of exploring the so-called "hard-sphere gas", a model system in which spheres interact only by mutual repulsion which forbids them from ever having a center-to-center distance smaller than twice their radius. These models are an ideal setting within which to explore excluded volume effects and do not suffer from the artificial constraint present in lattice models that force particles to only occupy a restricted set of points in space. We argue that the shortcomings in the model presented thus far are an artifact of the lattice model which result from the extremely approximate treatment of the volume exclusion. Studies of the hard-sphere gas have resulted in more sophisticated partition functions than that derived using a lattice model and result in the pressure of a hard sphere gas as a function of its concentration of the form

$$p = k_B T [H](1 + x + 0.625x^2 + 0.287x^3 + 0.110x^4). \tag{14.11}$$

This formula was first obtained by Boltzmann in 1899. The variable $x$ is defined as $x = 4V[H]$, where $V$ is the volume of a single hard sphere. This result of using the hard-sphere analysis is shown in fig. 14.11 and gives a much better result as the reader is asked to work out in the problems at the end of the chapter. The simple hard sphere gas description of a concentrated hemoglobin solution gives a quantitative explanation of the observed osmotic pressure.

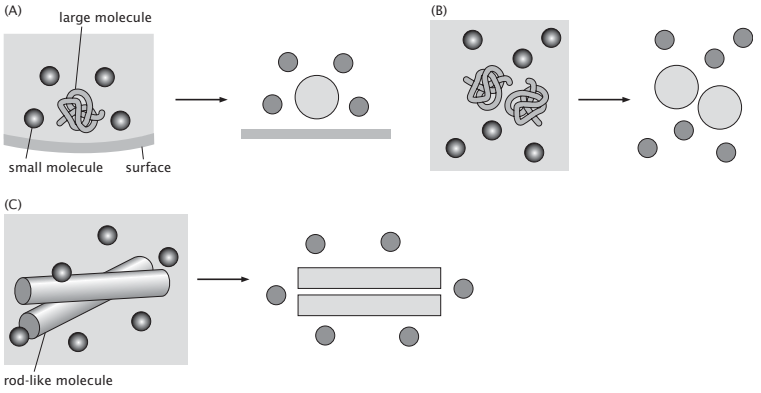


Figure 14.12: Schematic of the forces resulting from volume exclusion. In each of the schematics we show a two-dimensional idealization of the configuration of interest. (A) Large particle near a surface, (B) two large particles in solution, (C) two rod-like molecules in solution. As the two large objects come closer together, the total volume they exclude for the small disks decreases, resulting in an effective attractive force between the large particle and the surface, the two large particles, and the two rod-like molecules, respectively.

### 14.2.3 Depletion Forces: Order from Disorder

#### The Close Approach of Large Particles Excludes Smaller Particles Between Them, Resulting in an Entropic Force

One of the most intriguing and counterintuitive results of crowding is the way in which entropy can induce forces and structural ordering. A beautiful effect that arises on strictly entropic grounds is that of depletion forces, illustrated in fig. 14.12. The idea is that in a solution consisting of some large molecules (or particles) in the presence of some much smaller particles, as the large particles approach one another with a distance comparable to the size of the smaller particles, they will exclude the smaller particles from the volume between them. As they get even closer, the volume available to the smaller particles will *increase*. This has the effect of inducing an entropic force of attraction between the large particles. Macromolecules and macromolecular complexes in the cell are typically separated by distances that are comparable to their size. As a result, this kind of force should enter into the discussion of how macromolecules in the cell interact.

To see how depletion forces arise, we begin with the case of a two-dimensional system of large and small disks in the presence of a surface as shown in fig. 14.13. The large disk has radius $R$ while the smaller disks have a radius $r$. In this idealized two-dimensional geometry, our interest is in computing the total area available to the small disks as a function of the distance $z$ between the large disk

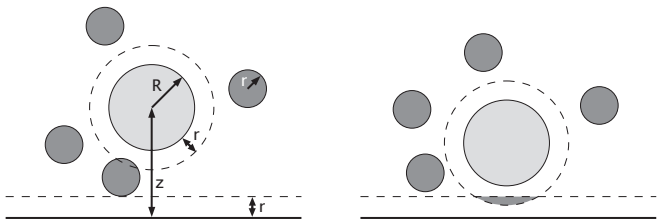


Figure 14.13: Geometry of excluded-volume interactions. A large disk of radius $R$ in the presence of a surface and multiple small disks of radius $r$. The dotted lines depict the volume excluded to the small disks. As the large disk approaches the surface, the total excluded volume for the small disks decreases due to the overlap of the volumes excluded by the large disk and the surface (depicted by dashed lines). This overlapping excluded volume is shown as the grey shaded region in the right figure. Because of the increase in the area available to the disks, there is an increase in their entropy and an effective attraction between the large disk and the surface.

and the surface. When the disk is far from the surface the total excluded area is the sum of the areas excluded by the disk and the surface. As the disk gets closer to the surface, there is a decrease in the area which is inaccessible to the small disks (shown as the shaded fragment of a circle) and this *increases* their entropy. The strategy of our calculations is then to compute the entropy of the small particles as a function of the distance between the large disk and the surface (or other interesting examples). This entropy will permit us to compute the free energy itself and once we have this free energy, we can compute $F = -\partial G/\partial z$ to obtain the effective depletion force between the disk and the surface. This calculation itself is given in the problems at the end of the chapter. At this point, we show how to consider these problems in general terms and then use the general formalism for a particular case study.

In the previous section we considered the crowding effect of one molecular species on the binding of another. We can use the same lattice model to build intuition about excluded-volume interactions. Formally, we consider a solution filled with two species, two large molecules in the presence of a large number of smaller crowding agents. We consider the situation in which there are no conventional forces (van der Waals, electrostatics, etc.) between the various molecules. Rather, the forces that arise do so strictly on the basis of the entropy changes incurred by close proximity of the two large molecules. In this situation the free energy of the small molecules will depend on the positions and

orientations (if the molecules have some structure to them) of the large ones. That is, the large molecules reduce the volume of space available to the small ones from $V_{\text{box}}$, the volume of the box, to $V_{\text{box}} - V_{\text{ex}}$, where $V_{\text{ex}}$ is the excluded volume. Concretely, the free energy change induced by this excluded volume is given by

$$G_{\text{ex}} = -Nk_BT \ln\left(\frac{V_{\text{box}} - V_{\text{ex}}}{v}\right) + Nk_BT \ln\left(\frac{V_{\text{box}}}{v}\right) \tag{14.12}$$

where $N$ is the number of small molecules and $v$ is a constant with units of volume (e.g., for a lattice model this would be the volume of a unit cell). This effect was already introduced in fig. 14.13 and is shown more precisely in fig. 14.14. Combining the two logarithms and assuming that the excluded volume $V_{\text{ex}}$ is much less than the overall volume of the box we can use the approximation $\ln(1+x) \approx x$, to obtain a simpler expression for this free energy as

$$G_{\text{ex}} = Nk_BT\frac{V_{\text{ex}}}{V_{\text{box}}} \ . \tag{14.13}$$

Note that the parameter $V_{\text{ex}}$ depends upon the distance between the two large molecules and hence that there will be a distant-dependent force. In particular, once the excluded volume regions of the two large particles begin to overlap this reduces $V_{ex}$ and increases the entropy of the small particles. In addition to its simplicity, eqn. 14.13 also has an appealing physical interpretation. We can identify $\frac{Nk_BT}{V_{\text{box}}}$ with the ideal-gas (osmotic) pressure of the small particles in the box, and therefore the excluded volume free energy is equal to the pressure-volume work done on the small-molecule gas in reducing the volume it occupies by $V_{\text{ex}}$.

To see how the calculations we have done thus far lead to depletion forces, consider a small change in the distance between the two large molecules. If this leads to a change in the free energy of the small molecules via eqn. 14.13 then we can interpret this as a depletion force between the two large molecules mediated by the small ones. The magnitude of this depletion force is simply the absolute value of the derivative of $G_{\text{ex}}$ with respect to the distance. The sign of the derivative indicates the direction of the force: if it is negative, $G_{\text{ex}}$ decreases with distance and the depletion force is repulsive, while a positive derivative indicates an attractive force.

To build quantitative intuition about the depletion interaction we consider the case of two large spherical particles in a sea of smaller spherical particles. As discussed in the previous paragraphs, the calculation of the depletion force boils down to determining the excluded volume $V_{\text{ex}}$. We first examine the case of two spheres of radius $R$ surrounded by smaller molecules of radius $r$.

The volume excluded by a single large sphere is a sphere of radius $R + r$. That is, the centers of the small spheres are unable to occupy any point within a distance of $R+r$ of the centers of the large spheres. If two spheres are present then the total volume excluded for occupancy by the small spheres is twice as large unless the distance between the spheres is such that their excluded

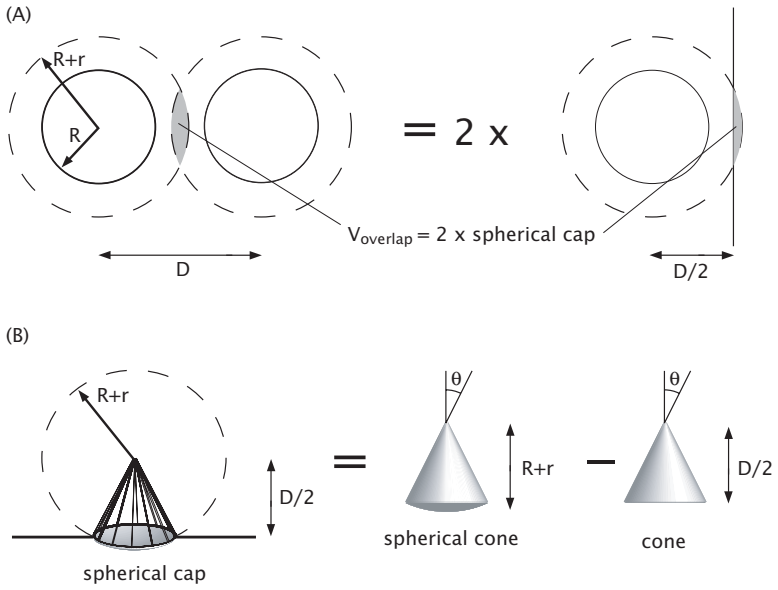


Figure 14.14: Depletion interaction between two spheres. (A) The depletion force is non-zero when two spheres come within a distance $D < 2(R + r)$, and is determined by the overlap volume which is twice the volume of a spherical cap. (B) The volume of a spherical cap is equal to the difference between the volume of a spherical cone and a cone.

volumes overlap. From the discussion above it should be clear that only in this case, when the distance between the two spheres, $D$, is less than $2(R+r)$, will there be an attractive depletion force between them. In this case the total excluded volume from both spheres is *less* than twice the excluded volume of each sphere individually and is given by

$$V_{\rm ex} = 2 \times \frac{4\pi}{3}(R+r)^3 - V_{\rm overlap} \ . \tag{14.14}$$

The overlap volume, shown in fig. 14.14(A), consists of two spherical caps whose volume can be computed by subtracting the volume of the spherical cone and that of the cone, as shown in fig. 14.14(B).

The volume of the spherical cone is given by the integral

$$V_{\rm spherical\ cone} = \int_0^{2\pi} d\phi \int_0^{\theta} \sin\theta\, d\theta \int_0^{R+r} r^2\, dr = \frac{2}{3}\pi(R+r)^3(1-\cos\theta). \tag{14.15}$$

Since $\theta$ is also the angle subtended by the cone we can replace its cosine by $\cos\theta = \frac{D/2}{R+r}$ to give

$$V_{\rm spherical\ cone} = \frac{2\pi}{3}(R+r)^2(R+r-D/2). \tag{14.16}$$

The volume of the cone is 1/3 of the volume of a cylinder with the same radius and height. The radius of the cone in fig. 14.14(B) is $\sqrt{(R+r)^2-(D/2)^2}$ and its height is $D/2$, therefore,

$$V_{\rm cone} = \frac{\pi}{3}(D/2)\left[(R+r)^2 - (D/2)^2\right]. \tag{14.17}$$

Finally we obtain the overlap volume as twice the difference between the volume of the spherical cone and the cone,

$$V_{\rm overlap} = \frac{2\pi}{3}(R+r-D/2)^2(2R+2r+D/2) \ . \tag{14.18}$$

To estimate the depletion force between the two large spheres we are left with taking the derivative of the free energy $G_{\rm ex}$ in eqn. 14.13 with respect to the distance $D$ which yields

$$F_{\rm depletion} = -\frac{\partial G_{\rm ex}}{\partial D} = -p\pi\left[(R+r)^2 - \frac{D^2}{4}\right] \ . \tag{14.19}$$

Here $p = nk_BT$ is the osmotic pressure of the small molecules ($n = N/V_{\rm box}$ is the concentration), and the distance between the two large spheres satisfies $2R < D < 2(R+r)$; for larger distances the overlap volume and the force are both zero. To get a feeling for the numbers, we take $R \gg r$ and $D \approx 2R+r$, in which case $F_{\rm depletion} \approx \pi n k_B T r R$. For a bead whose radius is $R = 1\ \mu$m surrounded by small molecules with $r = 2$ nm at a concentration $n = 1$ mM, the size of the depletion force is $F_{\rm depletion} \approx 15$ pN.

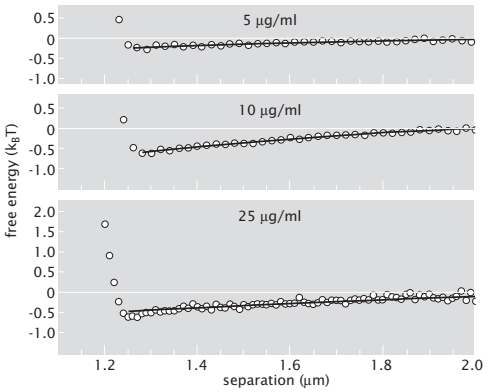


Figure 14.15: Measured free energies due to excluded volume. The free energy of interaction of two 1.25 $\mu$m diameter beads as a function of the concentration of the depleting agent (labeled in each panel). The depleting agent is mondisperse DNA from $\lambda$-phage with a radius of gyration of approximately 500 nm as measured using light scattering. (Adapted from A. G. Yodh *et al.*, Phil. Trans. R. Soc. Lond., A359:921, 2001.)

Depletion forces have been explored experimentally as shown in fig. 14.15. In the case shown in the figure, two beads of 1.25 $\mu$m diameter were confined to move along the line joining their centers. This confinement to one dimension was effected using an optical trapping system in which the laser is scanned so as to make a linear region in which the beads are trapped, but at constant potential. The depleting agent in the experiment is $\lambda$-phage DNA, 16 $\mu$m in length, which at concentrations shown in the figure forms spherical globules with a radius of roughly $r \approx 500$ nm. Polymer entropy in this case prevents overlap of different DNA molecules, so they effectively behave as hard spheres.

The experiment measures the distance between the beads using light microscopy. Repeated measurements of the distance lead to a determination of the probability distribution of distances, $p(D)$. Since in equilibrium $p(D)$ is proportional to the Boltzmann factor $\exp(-\beta G_{\rm ex}(D))$ then the logarithm of the measured distribution yields the free energy $G_{\rm ex}(D)$. This is the quantity plotted in fig. 14.15, for different DNA concentrations. (The free energy is determined up to a constant, which in the experiment was chosen so that $G_{\rm ex}(D)$ goes to zero at large $D$.)

The lines in fig. 14.15 are fits to the formula $G_{\rm ex}(D) = pV_{\rm overlap}$, where $V_{\rm overlap}$ is given by eqn. 14.18. The fitting parameters used were the effective radius of the DNA molecules ($r$ in eqn. 14.18) and the osmotic pressure ($p$). The effective radius of DNA was found to be concentration independent and its value consistent with independent measurements of the same quantity. The osmotic pressure, $p/k_BT$, was found to be proportional to the concentration of DNA, $n$, as van't Hoff's formula says, but with a coefficient of 0.5 instead of

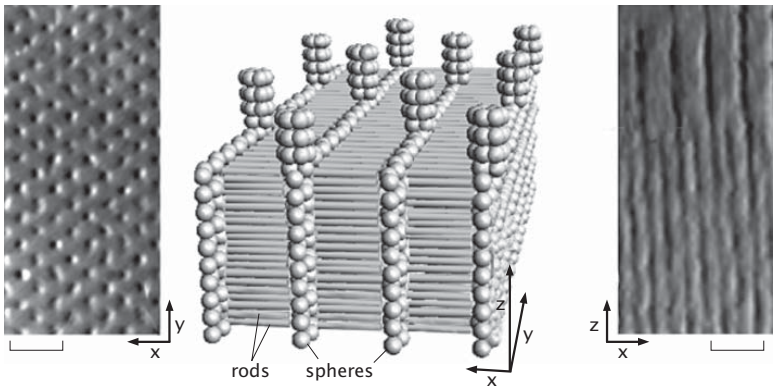


Figure 14.16: Entropic ordering of mixtures of hard rods and spheres. A solution of hard rods and spheres has a rich phase diagram that depends on the volume fractions of the two components, and it includes layered structures such as the one shown here. The left panel is a micrograph along the $z$ axis, while the one on the right was taken in the $y$ direction. The schematic in the middle depicts the proposed layered structure. The scale bars are 3 $\mu$m. (Adapted from M. Adams *et al.*, Nature, 393:349, 1998.)

1. The origins of this discrepancy are unclear and could be a source of further inquiry.

**Depletion Forces Can Induce Entropic Ordering!**

So far we have shown how excluded volume effects can lead to short-ranged, attractive depletion forces between two macromolecules. Beside the effect on bimolecular interactions, depletion forces can also produce ordered structures of surprising complexity. This is clearly seen in multicomponent systems such as the one made of filamentous viruses serving as hard rods and spheres, which produces the layered structures shown in fig. 14.16. The surprising thing about these structures is that entropy alone leads to microphase separation where layers of balls are interspersed with layers of rods. Macrophase separation, where the spheres and balls take up residence in different parts of the reaction volume, is the expected outcome, but experiments have shown that there are regions of phase space (determined by volume fractions of rods and spheres) where layered structures are preferred.

In light of these findings on model systems of rods and spheres, it is intriguing to consider whether depletion forces might be contributing to the organization of macromolecules and macromolecular complexes inside cells. As more quantitative data is obtained on the spatial arrangement of macromolecular complexes within cells, these questions might very well come to the forefront of physical biology.

### 14.2.4 Excluded Volume and Polymers

#### Excluded Volume Leads to an Effective Repulsion Between Molecules

Above we showed that the presence of small molecules in the solution can lead to an effective attraction between two larger molecules, by considering the volume that the large molecules exclude for the smaller ones. Here we take up the issue of the mutual exclusion of a collection of $N$ macromolecules confined to the interior of a cell, and each occupying a volume $v$. The excluded volume interaction refers to the effect that two molecules are not allowed to occupy the same location in the cell.

We adopt the lattice model used in section 14.2.2, where $N$ macromolecules are distributed among $\Omega$ boxes each of volume $v$. The excluded volume interaction manifests itself in the property that every box can be occupied by at most one macromolecule. To obtain an estimate of the effective repulsion between molecules due to the excluded volume interaction, we compute the free energy difference between the state where excluded volume is enforced and one in which it is not.

For the situation when the excluded volume is enforced the partition function is simply the number of ways of choosing $N$ boxes from the total number of boxes $\Omega$ in which to place the macromolecules. This is given by

$$Z_{\rm ex}(N) = \frac{\Omega!}{N!(\Omega - N)!} \ . \tag{14.20}$$

On the other hand, if we do not enforce the excluded volume condition the partition function is

$$Z_{\rm nex}(N) = \frac{\Omega^N}{N!} \ . \tag{14.21}$$

This amounts to saying that each of the $N$ macromolecules has $\Omega$ boxes to choose from regardless of whether the box is occupied or not. The $N!$ takes care of the fact that the macromolecules are regarded as identical.

Using the canonical relation between free energy and the partition function, $G = -k_B T \ln Z$, we can compute the free energy difference between the two states as

$$\Delta G_{\rm ex} = G_{\rm ex} - G_{\rm nex} = -k_B T \ln \frac{Z_{\rm ex}}{Z_{\rm nex}} \ . \tag{14.22}$$

To make further progress we make use of the Stirling approximation, $n! \approx (n/e)^n$, which is valid for $n \gg 1$ (described in "The Math Behind the Models" on pg. 280 and in the problems at the end of chap. 5). Within this approximation, the ratio of partition functions appearing in the above formula can be expressed as:

$$\frac{Z_{\rm ex}}{Z_{\rm nex}} = \frac{\Omega!}{\Omega^N(\Omega - N)!} \approx \frac{\left(\frac{\Omega}{e}\right)^\Omega}{\Omega^N \left(\frac{\Omega - N}{e}\right)^{\Omega - N}} = \frac{e^{-N}}{\left(1 - \frac{N}{\Omega}\right)^\Omega} \left(1 - \frac{N}{\Omega}\right)^N \ , \tag{14.23}$$

The reader is asked to explore the validity of the approximations we make in the problems at the end of the chapter. Assuming $\Omega \gg N$, we can use the formula $(1 - N/\Omega)^{\Omega} \approx e^{-N}$ to simplify the above equation to

$$\frac{Z_{\text{ex}}}{Z_{\text{nex}}} \approx \left(1 - \frac{N}{\Omega}\right)^{N} \quad . \tag{14.24}$$

Finally, if we plug this into eqn. 14.22 for the free energy difference due to the excluded volume effect, we find

$$\Delta G_{\text{ex}} = -N k_B T \ln\left(1 - \frac{N}{\Omega}\right) \approx k_B T \frac{N^2}{\Omega} \ , \tag{14.25}$$

where we have used the Taylor expansion for the logarithm ($\ln(1 - x) \approx -x$). Note that we can interpret the last formula by saying that the excluded volume interaction raises the free energy of the system of macromolecules by $k_B T \phi$ per molecule, where $\phi = N/\Omega$ is the volume fraction occupied by the macromolecules in the cell.

**Self-Avoidance Between the Monomers of a Polymer Leads to Polymer Swelling**

This chapter has argued that crowding reveals itself in many different ways. These effects can be observed experimentally, and also force us to reconsider many of the powerful theoretical tools developed so far in the book. In chap. 8 we developed the random walk model of polymers and have shown its utility in describing macromolecules such as DNA. One feature of the random walk model that is disturbing, however, is that it permits polymer configurations in which the monomers occupy the same position in space and the chain is allowed to self-intersect. Clearly these conformations are unphysical and one would be tempted to discard the random walk model on these grounds. Still we should remember that the random walk model is probabilistic in nature, and therefore, if the offending states are practically never realized (i.e. they have a vanishingly small probability), the model will provide reliable results for the average properties of flexible macromolecules. For example, if we are dealing with DNA whose length is only a few persistence lengths, then the energetic cost of making bends that would lead to self-intersections is too costly and will never happen. This observation begs the question, how long must a DNA molecule be before the self-avoidance effect starts rearing its head? For example, we have repeatedly used the formula $\sqrt{Na^2}$ for the size of a macromolecule such as DNA, which was derived based on the random walk model with no self-avoidance. We will demonstrate shortly that taking self-avoidance into account produces a very different result.

When can we ignore the self-avoiding property of polymers? To answer this question we make use of an estimate first suggested by Flory. The idea is to consider the competing effects of polymer chain entropy, which has the tendency to make the chain compact, and that of self-avoidance that tends to swell the chain up. To account for these two effects we start by writing down an

approximate expression for the free energy of the polymer chain as a function of its size $R$ as

$$G(R) = -TS_{\rm rw}(R) + G_{\rm ex}(R) \tag{14.26}$$

where $S_{\rm rw}(R)$ is the random-walk entropy for a chain of size $R$ and $G_{\rm ex}(R)$ is the excluded-volume interaction discussed above .

To estimate the entropy of the polymer chain we make use of the end-to-end distribution for a random walk, $P(R;N)$, given by eqn. 8.23 on page 401. In this case, we can write that result as

$$S_{\rm rw}(R) = k_B \ln P(R;N) + \text{const} = -k_B \frac{3R^2}{2Na^2} + \text{const} \tag{14.27}$$

where the constant term does not depend on the size ($R$) of the polymer chain.

For the excluded volume interaction ($G_{\rm ex}$) we approximate the polymer chain with a gas of hard cylinders of length $a$ ($a \approx 100$ nm is the Kuhn length for DNA) and diameter $d$ ($d \approx$ 2nm for DNA). Unlike the example treated previously, where we considered the excluded volume interaction for a gas of hard spheres, here we have to take into account that the volume that one cylinder excludes for the center of mass of another depends on their mutual orientation. As shown in fig. 14.17, for fixed orientation the excluded volume is estimated to be $v = 2da^2 \sin\theta$, where $\theta$ is the angle between the long axes of the cylinders. (The exact result for $v$ obtained by Onsager reduces to this formula for the case $a \gg d$.) Averaging of $\sin\theta$ over all possible orientation gives

$$\langle \sin\theta \rangle = \frac{1}{4\pi} \int_0^{2\pi} d\phi \int_0^{\pi} \sin^2\theta d\theta = \frac{\pi}{4} \tag{14.28}$$

to yield a final estimate for the excluded volume, $\pi a^2 d/2$. With this result in hand, we can adapt eqn. 14.25 to this situation. In order to use eqn. 14.25 in the form $G_{\rm ex} = k_B T N \phi$, we need to determine the volume fraction $\phi$. $N$ is the number of hard cylinders (i.e. the number of Kuhn segments that make up the polymer chain) and permits us to write the total volume fraction occupied by the cylinders making up the polymer chain as

$$\phi(R) = N \frac{\frac{\pi}{2} a^2 d}{\frac{4\pi}{3} R^3} = N \frac{3a^2 d}{8R^3}. \tag{14.29}$$

Eqn. 14.25 tells us how to construct the contribution of excluded volume to the free energy and results in

$$G_{\rm ex}(R) = k_B T N^2 \frac{3a^2 d}{8R^3}. \tag{14.30}$$

Putting the excluded-volume interaction term and the entropy term together, we arrive at the Flory estimate for the free energy of a polymer chain of size $R$, namely,

$$G_{\rm Flory}(R) = k_B T \frac{3R^2}{2Na^2} + k_B T N^2 \frac{3a^2 d}{8R^3} \ , \tag{14.31}$$

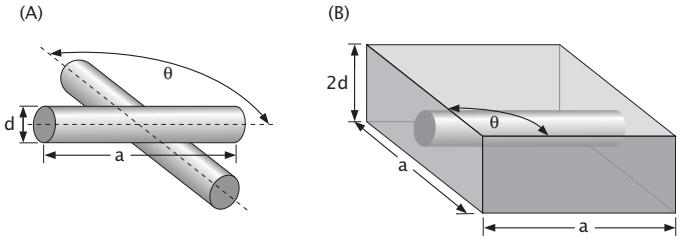


Figure 14.17: The excluded volume for two cylinders. (A) The volume that one cylinder excludes for another depends on their mutual orientation characterized by the angle $\theta$ between their long axes. (B) For the situation when the length of the cylinder is much greater than its diameter the excluded volume is well approximated by the shaded parallelepiped.

where we have dropped the unimportant constant term from the entropy estimate. To obtain the size of the polymer chain at equilibrium, all that remains is to determine that value of $R$ that minimizes the Flory free energy. This is accomplished by taking the derivative of eqn. 14.31 and setting it to zero, which yields

$$R_{\text{Flory}} = \left(\frac{3}{8}a^4 d\right)^{\frac{1}{5}} N^{\frac{3}{5}} \ . \tag{14.32}$$

Most notably, the size of the polymer with self-avoidance scales with the number of segments $N$ to the power $3/5$. The fact that this number is greater than $1/2$, the exponent associated with simple random walks, attests to the swelling of the chain induced by the excluded-volume interaction.

Given the radically different prediction for the size of a chain that inclusion of the self-avoidance term leads to, we might be tempted to discard all the estimates made previously based on the random walk model. This is not warranted, since for short enough polymers the self-avoidance can be ignored. To see this, lets compare the size of the self-avoidance interaction term, $G_{\text{ex}}(R)$, and the entropy term, $S_{\text{rw}}(R)$, in $G_{\text{Flory}}$ assuming that the size of the polymer is given by the random walk result $R = \sqrt{Na^2}$. In this case,

$$G_{\text{ex}} = k_B T \frac{3}{8}\frac{d}{a} N^{\frac{1}{2}} \tag{14.33}$$

and

$$S_{\text{rw}} = \frac{3}{2} k_B T \ , \tag{14.34}$$

follow from eqn. 14.30 and eqn. 14.27, respectively. We see that for $N$ large enough the self-avoidance interaction term will always dominate. Still, taking the parameter values appropriate for DNA, $d = 2$ nm and $a = 100$ nm, we can conclude that for $N \ll 16(a/d)^2 = 40,000$ the self-avoidance term will be much less than the random-walk entropy term and it can be safely ignored. This

many Kuhn segments of DNA corresponds to a molecule which is $L = Na = 40,000 \times 100$ nm, or 4 mm, in length. This is much larger than the length of the $\lambda$-phage genome $L \approx 16\mu$m, for example, indicating that for this long a strand of DNA self-avoidance can be safely ignored.

## 14.3 Crowded Dynamics

So far, we have examined how equilibrium properties are altered by the presence of crowding. However, as mentioned at the beginning of the chapter, a second way in which crowding is revealed is through changes in the dynamics within cells. In light of the observation of the possible importance of macromolecular crowding in producing new physical effects, we now return to some of the questions presented earlier in the present chapter concerning the nature of diffusion, but now from the point of view of the nature of the dynamics when the diffusive medium is dense and complex.

### 14.3.1 Crowding and Reaction Rates

#### Enzymatic Reactions in Cells Can Proceed Faster Than the Diffusion Limit Using Substrate Channeling

In dilute, *in vitro* biochemical experiments, the reaction rate for an enzymatic conversion of a substrate into a product depends upon the concentration of the enzyme, the concentration of the substrate and the intrinsic turnover rate of the enzyme. It is generally accepted that the concentration dependence of these rates describes the time it takes for an enzyme diffusing freely in solution to randomly encounter one another. At higher concentrations of either, these random collisions become more frequent.

Inside of cells, enzymes are rarely free to diffuse as they would in dilute solution since proteins tend to form large complexes or associate with membranes or cytoskeletal elements. One example of this effect can be seen in fig. 14.4 where it is shown that the glycolytic enzyme, phosphoglycerate kinase has an effective diffusion coefficient in cells that is roughly five times lower than GFP despite the fact that the two molecules are nearly the same size. We might expect then that reaction rates inside cells would be largely dominated by substrate concentration, however, in many critical metabolic pathways such as the Krebs cycle operating inside of mitochondria, the concentration of small molecule substrates such as the intermediate oxaloacetate is much too low to account for the overall flux through the metabolic pathway.

How can a cell drive an enzymatic transformation more rapidly than the physical law of diffusion should allow? One common solution, which may prove to be nearly universal, is that cells simply do not allow substrate molecules that are intermediates in metabolic pathways to diffuse from the active site of one enzyme in the pathway to the next. Instead, specific, though low-affinity, protein-protein interactions among all the enzymes in the pathway are used to

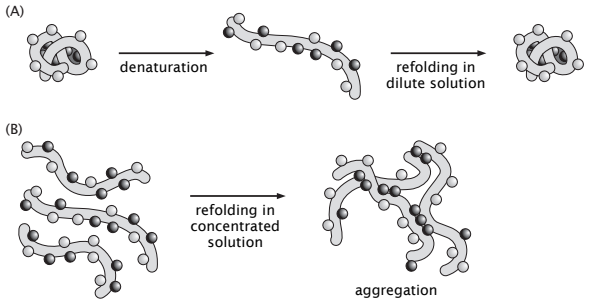


Figure 14.18: Protein folding and aggregation. A protein folded in its native state sequesters hydrophobic domains on the inside to hide the hydrophobic core. Denaturation disrupts the native structure exposing these hydrophobic patches. (A) When the protein is allowed to refold in very dilute solution, the hydrophobic patches within a single molecule self-associate to reform the native, hydrophobic core. (B) At high concentration, the hydrophobic patch of one protein molecule may associate with the hydrophobic patch of another triggering protein aggregation rather than native refolding.

assemble a giant, multi-enzyme complex in which the substrate can travel directly from the active site of one enzyme to another without ever freely diffusing. This behavior is known as substrate channeling.

Because of this effect, it is extremely challenging to predict the actual rate of a biochemical transformation *in vivo*, even if the concentration of both substrate and enzyme are known and the turnover rate of the enzyme has been accurately measured.

**Protein Folding Is Facilitated by Chaperones**

Another case where dilute, *in vitro* biochemical experiments fail to accurately represent the complexities of protein behavior inside of cells is in the study of protein folding. For many small proteins of relatively simple structure, they can be purified and denatured with harsh chemical agents such as urea or guanidinium hydrochloride. When the denaturing agents are removed, the proteins will refold *in vitro* to their original native structure. These kinds of experiments are successful only when the protein concentration is several orders of magnitude lower than the actual concentrations of protein inside of cells. In more crowded solutions, denatured proteins tend to aggregate by intermolecular association of their hydrophobic patches or domains preventing proper intramolecular association of these domains to form the protein's hydrophobic core as shown in fig. 14.18.

How do cells prevent aggregation of proteins as they are synthesized from

ribosomes in the highly crowded cytoplasmic environment? Specialized proteins called chaperones facilitate protein folding both by increasing its rate and by preventing aggregation of partially folded protein intermediates. These chaperones come in two flavors. Chambered chaperones such as GroEL in bacteria and TRiC in eukaryotic cells actually form a tiny private room in which an individual polypeptide chain is free to fold with no danger of random collision with the hydrophobic patches of others. These chambered chaperones consume ATP in the process of opening and closing the door to the room. The second class of chaperone exemplified by small heat-shock proteins such as HSP70 tend not to require ATP for their action. These bind to the hydrophobic domains of nascent proteins as they emerge from the ribosome and prevent their aggregation until the entire protein domain has been translated and is ready to fold.

### 14.3.2 Diffusion in Crowded Environments

As was already illustrated in figs. 14.4 and 14.5, diffusion in crowded environments is more subtle than its dilution-solution counterpart. Theoretical responses to this challenging question are usually all built around the same fundamental and intuitive idea: for a particle to hop to a new position, that new position cannot already be occupied. A simple random walk model can be used to illustrate the effect of crowding on molecular diffusion, though we note that like with the treatments earlier in the chapter, this is only a modest attempt to come to terms with the problem. To make the model concrete, assume that the volume fraction occupied by the molecules is $\phi$ and that no two molecules can occupy the same site. In this case the probability that a chosen site is occupied by a molecule is $\phi$. Further, for simplicity, we consider only a one-dimensional walker.

The random walk now proceeds in the usual way: at every time instant $\tau$ the particle makes a jump to the left or to the right with equal probability. The jump is successful only if there is no particle at the new location. Therefore the particle jumps to the right, or to the left, with probability

$$p_{\text{right}} = p_{\text{left}} = \frac{1}{2} \times (1 - \phi) \tag{14.35}$$

where $1/2$ is the probability for attempting the jump, while $1 - \phi$ is the probability that the new site is unoccupied, thus allowing for a successful completion of the jump. If the neighboring site is occupied the attempted jump will be unsuccessful and the particle will stay put. The probability of that outcome is equal to the probability that a neighboring site is occupied which results in

$$p_{\text{stay}} = \phi \tag{14.36}$$

which is also equal to $1 - p_{\text{jump}}$. These three possible outcomes are illustrated in fig. 14.19

To compute the diffusion constant associated with this random walk we evaluate the mean square displacement $\langle x^2 \rangle$ as a function of time $t$. For $t = \tau$

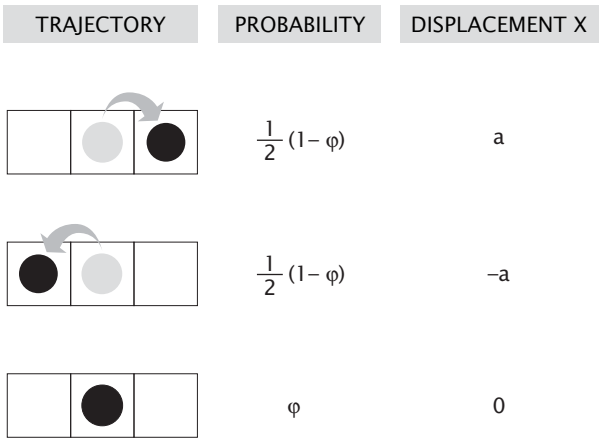


Figure 14.19: Trajectories and weights for a one-dimensional random walk which takes into account the effect of crowding.

the trajectory consists of a single step and

$$\left\langle x^2 \right\rangle (\tau) = a^2 \times p_{\text{right}} + a^2 \times p_{\text{left}} + 0 \times p_{\text{stay}} = a^2(1-\phi) \ . \tag{14.37}$$

After time $t$ the molecule makes $N = t/\tau$ steps and the mean square displacement is $N$ times larger than that in eqn. 14.37,

$$\left\langle x^2 \right\rangle (t) = \frac{t}{\tau} \times \left\langle x^2 \right\rangle (\tau) = \frac{a^2}{\tau}(1-\phi)t \ . \tag{14.38}$$

As we did in Chapter 13, we read off the diffusion constant from eqn. 14.38, and

$$D = D_0(1-\phi) \tag{14.39}$$

where $D_0 = a^2/2\tau$ is the result we obtained for the diffusion constant of a random walker when no other molecules are present.

We see that the effect of crowding is to reduce the diffusion constant by an amount proportional to the volume fraction occupied by the molecules. This will in turn affect the diffusion limited on-rate. Several examples of measurements on diffusion both of tracer molecules and of self-diffusion are shown in fig. 14.20. Qualitatively, it is seen that the model results are consistent with the trends revealed by the data. On the other hand, the precise functional form yielded by the model is based upon a coarse, "mean field" description and a more sophisticated treatment based on excluded volume of hard spheres provides a semiquantitative explanation of the data (see Muramatsu and Minton, 1988 for details).

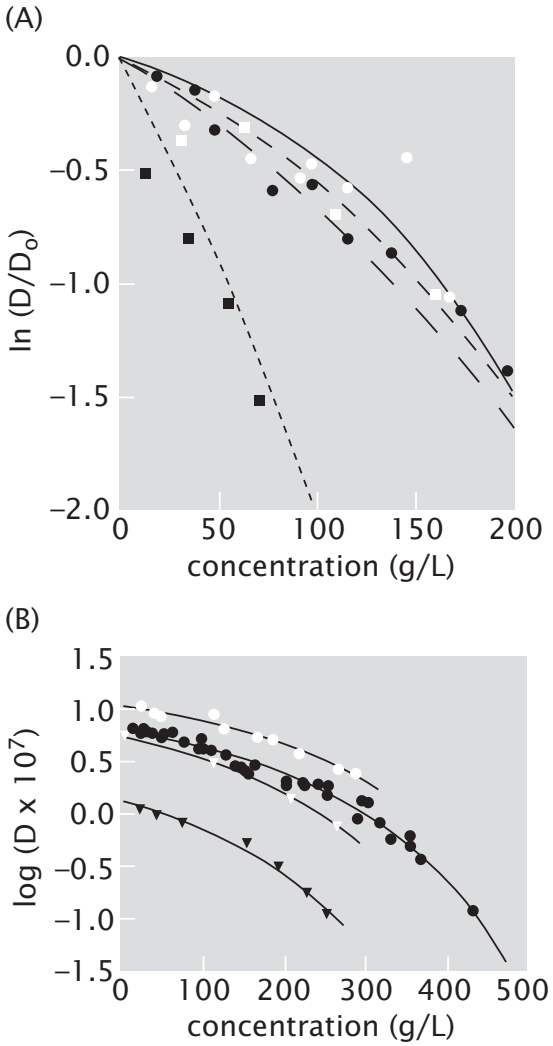


Figure 14.20: Diffusion and crowding. (A) Tracer diffusion as a function of protein concentration. FITC-aldolase diffusing in background of aldolase (open circles), BSA (filled circles), ovalbumin (open squares) and ribonuclease (filled squares). (B) Self-diffusion of globular proteins as a function of the protein concentration. Myoglobin (open circles), hemoglobin (filled circles), ovalbumin (open triangles), invertebrate hemoglobin (filled triangles). (A, adapted from N. Muramatsu and A. P. Minton, Proc. Nat. Acad. Sci., 85:2984, 1988; B, adapted from S. B. Zimmerman and A. P. Minton, Annu. Rev. Biophys. Biomol. Struct., 22:27, 1993.)

## 14.4 Summary and Conclusions

This chapter has explored one of the exciting frontiers at the interface between cell biology and physical theory, namely, how the properties of living matter differ from conventional solutions as a result of their extreme crowding. We have examined two broad classes of consequences: i) how equilibrium reactions are altered, ii) how dynamics of diffusion and biochemical rates are altered. Though this chapter appears in the part of the book entitled "Life in Motion", the alert reader will notice that the majority of our calculations have centered on equilibrium phenomena. This is a reflection of our inability to put together a compelling set of simple models that respond to the interesting data on crowding.

## 14.5 Problems

**1. A Feeling for the Numbers: Comparing *in vitro* and *in vivo* concentrations.**

In the chapter, we argued that the mean spacing between molecules in an *in vitro* biochemical experiment is roughly 100 nm at mM concentrations while in the cell the spacings are a factor of ten smaller. Justify these statements with simple estimates. The biochemical "standard state" is often taken as 1 M. Work out the mean spacing between molecules at this concentration.

**2. Effective concentrations and activity.**

The effect of crowding on the chemical potential of a molecular species in solution can be captured by the equation $\mu = \mu_0 + k_B T \ln\left(\frac{c\gamma}{c_o}\right)$, where the subscripts zero are for a reference state. The effective concentration is given by $c\gamma$, where $c$ is the actual concentration that is present in the solution and $\gamma$ is called the activity coefficient. The simple toy model of binding in the presence of crowders introduced in the chapter implies a corresponding model for the activity coefficient. Work out this activity coefficient and compare your formula to the experimental results shown in fig. 14.21.

**3. Osmotic pressure of hemoglobin**

Use the approximate formula for the pressure of a gas of hard spheres, eqn. 14.11, to extract an effective hard sphere radius for hemoglobin from the data given in fig. 14.11. How does this effective radius compare to the dimensions of the molecule obtained by X-ray scattering?
Relevant data for this problem is provided on the book website.

**4. Depletion force between a sphere and a surface.**

Compute the depletion force between a sphere of radius $R$ and a planar surface by carrying out the calculation indicated schematically in fig. 14.13. The radius of the small spheres is $r$.

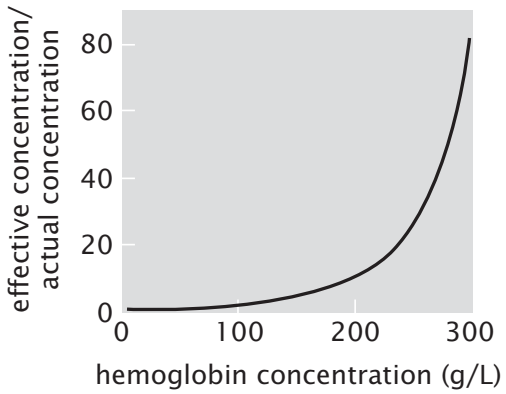


Figure 14.21: Crowding and the activity coefficient. Effect of hemoglobin concentration on its effective concentration. (Adapted from A. P. Minton,**J. Biol. Chem.** 275:10577, 2001.)

**5. Excluded Volume Interactions** In the chapter we worked out a general statement of the free energy for two large objects in solution and in the presence of small depletant molecules, which was based upon the osmotic pressure of the molecules and the volume excluded by the objects when at distance $D$. Repeat that derivation leading up to the formula

$$G(D) = \Pi_o V_{\rm ex}(D), \tag{14.40}$$

where $\Pi_o = Nk_BT/V$ is the osmotic pressure of the depletant molecules. Then, make an estimate of what this osmotic pressure is by using the concentration of proteins inside of a cell like *E. coli*. To figure that out, use the fact that such a cell has a volume of about 1 $\mu m^3$ and roughly $2 \times 10^6$ proteins in its cytoplasm. Using this value for $\Pi_o$ and the excluded volume between two spheres of radius $1\mu m$, work out the force as a function of distance and make a plot using pN as your unit of force and nm as your unit of distance. Assume that the small depletant molecules have a radius of 3 nm.

**6. Self-avoidance in flatland.** Repeat the Flory calculation from the chapter (sec. 14.2.4) for DNA confined to a two-dimensional surface.
(a) Find the scaling of the size of the polymer as a function of its length incorporating self-avoidance.
(b) Estimate the DNA length for which self-avoidance becomes important. How does this compare to the length of genomic DNA from a $\lambda$-phage?

**7. Diffusion and crowding.**

In this problem we extend the one-dimensional model of diffusion in the presence of crowding molecules (see pg. **??**) to account for the difference in size

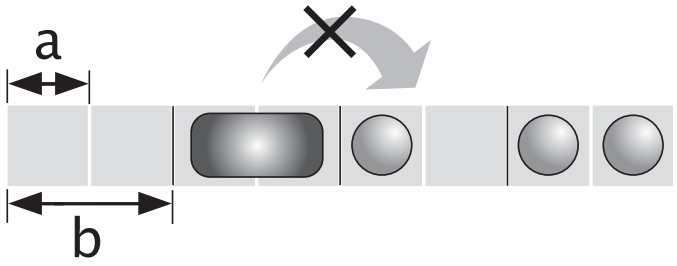


Figure 14.22: Lattice model of tracer particles of size $b$ diffusing in the presence of crowding molecules of size $a$. The tracer particle can hop to the neighboring tracer site only if there are no crowding molecules present in the $r = b/a$ adjacent crowding molecule sites. The fraction of sites occupied by crowding molecules is $\phi$.

between a tracer particle (considered to be present at low concentration) and the crowders. This situation is relevant for the data shown in fig. 14.20(A). The tracer particles are assumed to be undergoing random walk motion on the larger tracer lattice with lattice constant $b$, while the crowders are hopping between adjacent sites of the smaller lattice, with lattice constant $a$ (see fig. 14.22). The two lattices are introduced to account for the difference in size between the two molecular species.

(a) Calculate the diffusion coefficient by considering the possible trajectories, and their probabilities, of the tracer particle. Note that the tracer can hop to an adjacent site of the tracer lattice only if there are no crowders present. Express your answer in terms of the diffusion coefficient $D_0$ of the tracer particles in the absence of crowders, the volume fraction of the crowders $\phi$, and the ratio of the tracer and crowder sizes $r = b/a$.

(b) Plot $\ln D/D_0$ as a function of the volume fraction for different values of $r$. How well does this model explain the data shown in fig. 14.20(A)? To make this comparison you will need to estimate the sizes of the molecules used in the experiment from their molecular masses and a typical protein density which is 1.3 times that of water. The data is provided on the book Web site.

## 14.6 Further Reading

D. S. Goodsell, **Our Molecular Nature**, Springer-Verlag, New York: New York, 1996. Goodsell's illustrations provide a compelling, visual demonstration of the extent of crowding in cells.

S. B. Zimmerman and A. P. Minton, "Macromolecular Crowding: Biochemical, Biophysical and Physiological Consequences", Annu. Rev. Biophys. Biomol. Struct. **22**, 27 (1993). Classic article that raises many of the important issues

associated with "crowding".

K. Luby-Phelps, "Cytoarchitecture and Physical Properties of Cytoplasm: Volume, Viscosity, Diffusion, Intracellular Surface Area", Int. Rev. Cytology **192**, 189 (2000). This article spells out the key hidden assumptions in biochemistry.

A. P. Minton, "The Influence of Macromolecular Crowding and Macromolecular Confinement on Biochemical Reactions in Physiological Media", J. Biol. Chem. **276**, 10577 (2001). This paper lays out many of the interesting issues that arise as a result of the crowded environment in cells.

R. J. Ellis, "Macromolecular crowding: obvious but underappreciated", Trends in Biochem. Sci. **26**, 597 (2001). A very useful introduction to the subject of crowding and its relevance to both equilibrium phenomena and kinetics.

D. Bray, **Cell Movements: From Molecules to Motility**, Garland Publishing, New York: New York, 2001.

S. Asakura and F. Oosawa, "Interaction between Particles Suspended in Solutions of Macromolecules", J. Polymer Sci. **33**, 183 (1958). A beautiful example of theoretical reasoning to predict new phenomena. The authors note that "experimental proof of the reality of force derived here has not yet been obtained", a reminder that theoretical ideas can be useful even without the so-called "supporting data".

P. G. de Gennes, **Scaling Concepts in Polymer Physics**, Cornell University Press, Ithaca: New York, 1979. de Gennes gives a clear derivation of the role of excluded volume effects in polymers.

## 14.7 References

M. Adams, Z. Dogic, S.L. Keller, and S. Fraden, "Entropically driven microphase transitions in mixtures of colloidal rods and spheres", Nature **393**, 349 (1998).

D. H. Burk and Z. H. Ye, "Alteration of oriented deposition of cellulose microfibrils by mutation of a katanin-like microtubule-severing protein", Plant Cell, **14**, 2145 (2002).

A. D. Douglass and R. Vale, "Single-molecule microscopy reveals plasma membrane microdomains created by protein-protein networks that exclude or trap signaling molecules in T cells", Cell **121**, 937 (2005).

N. Hirokawa, "Cross-linker system between neurofilaments, microtubules, and membranous organelles in frog axons revealed by the quick-freeze, deep-etching method", J Cell Biol., **94**, 129 (1982).

T. C. Jarvis, D. M. Ring, S. S. Daube and P. H. von Hippel, ""Macromolecular crowding": thermodynamic consequences for protein-protein interactions within the T4 DNA replication complex", J. Biol. Chem. **265**, 15160 (1990).

A. Kornberg, "Ten Commandments: Lessons from the Enzymology of DNA Replication", J. Bacteriol. **182**, 3613 (2000).

S. O. Meroueh, K. Z. Bencze, D. Hesek, M. Lee, J. F. Fisher, T. L. Stemmler and S. Mobashery, "Three-dimensional structure of the bacterial cell wall peptidoglycan", Proc. Nat. Acad. Sci. **103**, 4404 (2006).

K. Mitra, I. Ubarretxena-Belandia, T. Taguchi, G. Warren and D. M. Engelman, "Modulation of the bilayer thickness of exocytic pathway membranes by membrane proteins rather than cholesterol", Proc. Nat. Acad. Sci. **101**, 4083 (2004). Table 1 of this paper gives a useful list of protein to phospholipid mass ratios for a number of different membranes.

N. Muramatsu and A. P. Minton, "Tracer diffusion of globular proteins in concentrated protein solutions", Proc. Nat. Acad. Sci., **85**, 2984 (1988).

P. P. Provenzano, K. Hayashi, D. N. Kunz, M. D. Markel and R. Vanderby, "Healing of subfailure ligament injury: comparison between immature and mature ligaments in a rat model.", J. Orthop. Res., **20**, 975 (2002).

P. D. Ross and A. P. Minton, "Analysis of Non-ideal Behavior in Concentrated Hemoglobin Solutions", J. Mol. Biol. **112**, 437 (1977).

T. M. Svitkina, A. B. Verkhovsky, K. M. McQuade and G. G. Borisy, "Analysis of the actin-myosin II system in fish epidermal keratocytes: mechanism of cell body translocation", J. Cell Biol., **139**, 397 (1997).

T. M. Svitkina, E. A. Bulanova, O. Y. Chaga, D. M. Vignjevic, S.-I. Kojima, J. M. Vasiliev and G. G. Borisy, "Mechanism of filopodia initiation by reorganization of a dendritic network", J. Cell Biol., **160**, 409 (2003).

A. S. Verkman, "Solute and macromolecule diffusion in cellular aqueous compartments", Trends Biochem. Sci. **27**, 27 (2002).

A. G. Yodh, K.-H. Lin, J. C. Crocker, A. D. Dinsmore, R. Verma and P. D. Kaplan, "Entropically driven self-assembly and interaction in suspension", Phil. Trans. R. Soc. Lond. **A359**, 921 (2001).